scientific reports

Check for updates

OPEN

An investigation on structural, optical, and magnetic properties of $Zn_{1-x}Co_xO$ nanorods fabricated by electrochemical deposition

Mansour Mohamed[1], A. Sedky[2]✉, Abdullah S. Alshammari[1], M. Bouzidi[1], Z. R. Khan[1] & Marzook S. Alshammari[3]

We reported here the structural, optical, and magnetic properties of $Zn_{1-x}Co_xO$ nanorods (NRs) with x = 0.00, 0.025, 0.05, and 0.30 wt%. The $Zn_{1-x}Co_xO$ NRs samples were fabricated by electrochemical deposition and given the symbols S0, S1, S2, and S3 for x = 0.00, 0.025, 0.05, and 0.30 wt%, respectively. It is found that all NR samples were grown along the (002) plane and have a hexagonal structure. As the Co level increases up to 0.30 wt%, the crystallite size and the texture coefficient are respectively decreased from 57 nm to 0.98 to 25 nm and 0.70. While the diameter of NRs increased from 347 to 1730 nm. Interestingly, the weight% (wt %) of O was increased with increasing Co level. The optical band gap (E_g) was found to be 3.32 eV for the undoped ZnO NRs (S0) and reduced to 2.24 eV with more increase of Co up to 0.30 wt%. At 300 K, the So and S1 exhibit diamagnetic behavior over the field range. For S2, such behavior became weakly ferromagnetic at H ≤ 2000 Oe and diamagnetic at H > 2000 Oe. In contrast, the S3 exhibits strong ferromagnetic behavior of magnetization (M) = 0.14 emu/g at 20 kOe. However, with decreasing temperature to 10 K, the paramagnetic behavior is dominant for all NRs. However, all NRs samples revealed a hysteresis loop After subtracting the paramagnetic and diamagnetic contributions from the M-H curves. The S2 showed the highest value for coercive field of 256 and 263 Oe, as compared to the other NRs (15–65 Oe). Although S3 shows the softest magnetic properties among all samples (with coercive fields of 15–27 Oe), it exhibits the strongest ferromagnetic behavior. The Zfc/Fc measurements show that all the samples are paramagnetic by nature with no sign for blocking temperature of magnetic nanoparticles. Furthermore, the residual magnetization values measured at 300 K (from both FC and ZFC curves) show a general increasing trend with cobalt doping concentration, with measured values of 6.45×10^{-9}, 2.13×10^{-4}, 8.71×10^{-5}, and 6.45×10^{-2} emu/g for samples S0 through S3, respectively. This work provides new insights into the correlation between electrochemical growth conditions, defect chemistry, and room-temperature ferromagnetism in Co-doped ZnO systems, advancing beyond previous reports through its demonstration of bandgap tuning and robust ferromagnetism in electrochemically grown NRs and temperature-dependent magnetic phase transitions directly correlated with structural parameters.

Keywords ZnO, nanorods, Electrochemical deposition, Ferromagnetic, Spintronics

ZnO is a semiconductor with unique chemical and physical properties, large exciton binding energy (60meV), and broad band gap E_g (3.2 eV)[1]. Because of these characteristics, ZnO is a viable option for a number of uses, such as photocatalysis, optoelectronics, and sensors[2]. Doping, on the other hand, can greatly improve its intrinsic features by adding foreign atoms to the ZnO lattice, changing its optical, magnetic, and electrical characteristics[3–6]. Doping ZnO with transition magnetic elements like Ni, Co, Mn, and Fe has garnered significant attention due to its potential to induce room-temperature ferromagnetism (RTFM), a highly sought-after characteristic for spintronic devices[7–11].

[1]Department of Physics, College of Science, University of Hail, P.O. Box 2440, Hail, Saudi Arabia. [2]Department of Physics, Faculty of Science, Assiut University, Assiut 71516, Egypt. [3]Microelectronics and Semiconductors Institute, Energy and Industry Sector, KACST, Riyadh, Saudi Arabia. ✉email: sedky196000@hotmail.com

On the other hand, on the nanoscale, the magnetic properties of materials often differ markedly from those in their bulk form[8,9]. Among these nanoscale materials, nanorods (NRs) have attracted considerable interest in the field of magnetism due to their distinct characteristics and potential applications[12–16]. Their high surface area-to-volume ratio can significantly enhance magnetic properties. Additionally, their NRs -like shape induces shape anisotropy, resulting in unique magnetic behaviors that are not observed in the other spherical nanoparticles[6,12,15,17–24]. This anisotropy can be leveraged to customize magnetic properties for specific applications[20,23,25,26]. Several studies have been reported on the origin of RTFM in pure and doped ZnO nanorods. For instance, the FM features of undoped ZnO NRs, synthesized by chemical method under vacuum conditions, have attributed to both oxygen vacancies (Ov) and the large surface area (SA) of the NRs[27]. Modification of ZnO by doping or composite of another oxide has been widely used, for example, to achieve enhanced SA and Ov, reduce particle size (PZ), increase the number of active surface sites, reduce electron-hole recombination, and increase charge transfer processes, which may lead to tunable E_g and RTFM[28,29].

Co-ions are known to be one of the effective magnetic dopants that are frequently used for doping of various TMs oxides such as ZnO since the ionic radius of divalent Co^{2+} (0.065 nm) is smaller than that of Zn^{2+} (0.074 nm), which illustrates the feasibility of Co-ions substitution in ZnO. Cobalt oxide is generally recognized as a p-type semiconductor with several stable cubic phases, such as CoO, Co_2O_3, and Co_3O_4. It exhibits a broad range of direct bandgaps between 1.48 eV and 2.19 eV[30,31]. Therefore, it is possible to modify the properties of ZnO NRs through Co^{2+}ion incorporation. For example, the doping of ZnO with Co showed an improvement in the RTFM, whereas a further increase was associated with the quenching of RTFM[32]. Additionally, the E_g could gradually decrease with increasing Co concentration because of the sp-d exchange interactions between the free electrons of cations and the localized d-electrons of Co[33,34]. Although Co-ions are known as FM, their contribution to the development of RTFM in ZnO is still unclear. For more identification, the Co-doped ZnO NRs synthesized by co-precipitation showed RTFM, which have been assigned to be purely intrinsic[25]. In addition, an impurity phase has been found in the highly Co-doped ZnO nanorods, which caused a reduction of their magnetization of the fabricated NRs[25]. In addition, the studies on the magnetic properties of $Zn_{1-x}L_{ax}O$ NRs fabricated by chemical route have reported RTFM, which is caused by the formation of defects[6].

Previous studies have examined the structure and properties of $Zn_{1-x}Gd_xO$ nanorods across different doping levels (x)[35]. All samples exhibited a hexagonal wurtzite structure with well-defined nanorod morphology. In addition, a systematic evolution of RTFM of ZnO NRs with increasing x was observed. On the other hand, $Zn_{1-x}Co_xO$ NPs show anomalous anisotropic broadening for $x > 0.05$, which is due to a reduction in the particle size and strain contribution[36]. In addition, the presence of grouped Co^{2+} ions reveal the presence of clusters of high-spin Co^{2+} with antiferromagnetically coupled spins, which is responsible for the strain. On the other hand, effects of Ce doping (1–5%) on the ZnO NRs have been reported[37]. A hexagonal structure and NR nature could be confirmed for all NRs. The band gap was decreased gradually against Ce from 3.192 to 3.177 eV. The photoluminescence confirms the presence of intrinsic defects like Zn and Ov. A very weak ferromagnetic ordering was observed in all the NRs at RT. These findings recommend the NRs for the optoelectronic and spintronic devices.

Although several studies have investigated the magnetic properties magnetic properties of undoped and doped ZnO nanorods, the origin of RTFM in ZnO NRs still needs further investigation. Furthermore, based on the studies appearing in the literature, the growth conditions of NRs preparation can affect the dimensions as well as SA of the NRs and consequently control their magnetic properties[14,28,29]. Among the growth techniques used for the synthesizing of ZnO NRs is the electrochemical deposition, which is considered a low-cost technique and capable of producing uniform nanorods with a large SA[28,30,31]. Based on the above literature, while there have been many studies on Co-doped ZnO systems, researchers still face several challenges in this field. For example, it's difficult to precisely control how cobalt atoms distribute within the material during growth, and how the nanorod shape affects magnetic stability at room temperature. There's also much to investigate how changing the material's optical properties relates to its magnetic behavior. Our work tackles these questions by using optimized electrochemical method that produces highly uniform cobalt-doped nanorods, allowing us to systematically study how their structure affects their properties.

The objectives of this study are to fabricate ZnO NRs through the electrochemical deposition method. This research aims to thoroughly explore and discuss the structural, morphological, optical, and magnetic properties of the NRs, with particular emphasis on how cobalt doping and the nanoscale dimensions of the samples influence these characteristics. These comprehensive investigations will contribute to a deeper understanding of the properties and potential applications of ZnO NRs. Our results provide new clarity to the field by showing exactly how the growth conditions can prevent unwanted secondary phases and ensure proper cobalt incorporation into the crystal structure. We found specific relationships between how much cobalt is added and changes in both the material's bandgap and its magnetic properties at room temperature. These findings are particularly valuable for developing future applications in areas like spin-based electronics that need materials to perform reliably in demanding conditions.

Experimental procedures

$Zn_{1-x}Co_xO$ NRs were fabricated by electrochemical deposition technique using Autolab PGSTAT101 controlled with NOVA electrochemical software. The synthesizing of $Zn_{1-x}Co_xO$ NRs, with x = 0.00, 0.025, 0.05 and 0.30, was carried out in cell containing three electrodes; working electrode (ITO substrates), a reference electrode (Ag/AgCl in saturated KCl) and a counter electrode (platinum wire). Prior to the preparation experiments the glass cell and ITO substrates were cleaned by washing them several times in ultrasonic cleaner using isopropanol and deionized water. For fabrication the undoped samples the zinc nitrate hydrate ($Zn(NO_3)_26H_2O$,) and hexamethylenetetramine (HMT) were used as the starting materials. However, for synthesizing of the

doped samples (the $Zn_{1-x}Co_xO$ NRs) the zinc nitrate hydrate ($Zn(NO_3)_26H_2O$,), cobalt nitrate hexahydrate ($Co(NO_3)_2{\cdot}6\,H_2O$) and hexamethylenetetramine (HMT) were used as the starting materials.

These precursors were dissolved in 200 ml deionized water and then the solution was inserted in the three-electrode cell which is connected to PGSTAT101 controller using the potentiostatic mode. In this mode a potential of −1 V recorded by the Nova software, was applied to the cell. During the growth process the solution in the cell was stirred continuously using magnetic stirrer. The solution temperature was maintained at 80 ° C and all samples were grown at time of an hour. After the growth period concluded, the fabricated undoped and doped ZnO nanorods were removed from the growth cell, washed with distilled water, and then air-dried at room temperature. The samples with x = 0.00, 0.025, 0.05 and 0.30 given the symbols S0, S1, S2, S3, respectively. The structure, morphology and elemental composition of $Zn_{1-x}Co_xO$ NRs were examined using X-ray diffractometer (Model-1710), a FEI Quanta 250 SEM and energy dispersive X-ray (EDX), respectively. The optical measurements of the $Zn_{1-x}Co_xO$ NRs were recorded by double beam spectrophotometer (model). DC magnetization measurements are performed using a SQUID magnetometer (Quantum Design MPMS 3) with an applied field up to 20 kOe, high sensitivity of 10^{-8} emu, a magnetic field of 7 Tesla, and a temperature range between 2 and 400 K. Additionally, magnetization as a function of temperature (10–300 K) is measured in both field cooling (FC) and zero-field cooling (ZFC) conditions at a field of 100 Oe. Specifically, the samples are first cooled to 10 K without the field; then the field is applied, and data are collected as the temperature increases to 300 K (ZFC). Subsequently, the samples are cooled again, and FC magnetization is measured in the presence of the field. To isolate the intrinsic magnetic behavior of the NRs, both paramagnetic and diamagnetic contributions are subtracted from the M-H curves.

Results and discussion

Morphology and structural properties

Figure 1 shows the measured SEM images taken for $Zn_{1-x}Co_xO$ NRs. The surface of ITO substrates is fully covered with hexagonal nanorod-like structures corresponding to the typical structure of ZnO crystal. It is observed that the great influence of the addition of Co ions on the host material (ZnO) is such that the shape and dimensions of the NRs are affected. Figure 2 shows the nanorod diameter against the Co content. The solid curve in the figure represents a non-physical guide for the eye only, connecting discrete data points. No continuous functional relationship is implied. As seen in Fig. 2; Table 1 the diameter of the NRs is increased from 347 to 1730 nm by increasing Co content because the rate of growth along the transvers axis is higher than that of longitudinal one. And this could be explained in terms of the diffusion of Zn^{2+} and Co^{2+} ions and generation

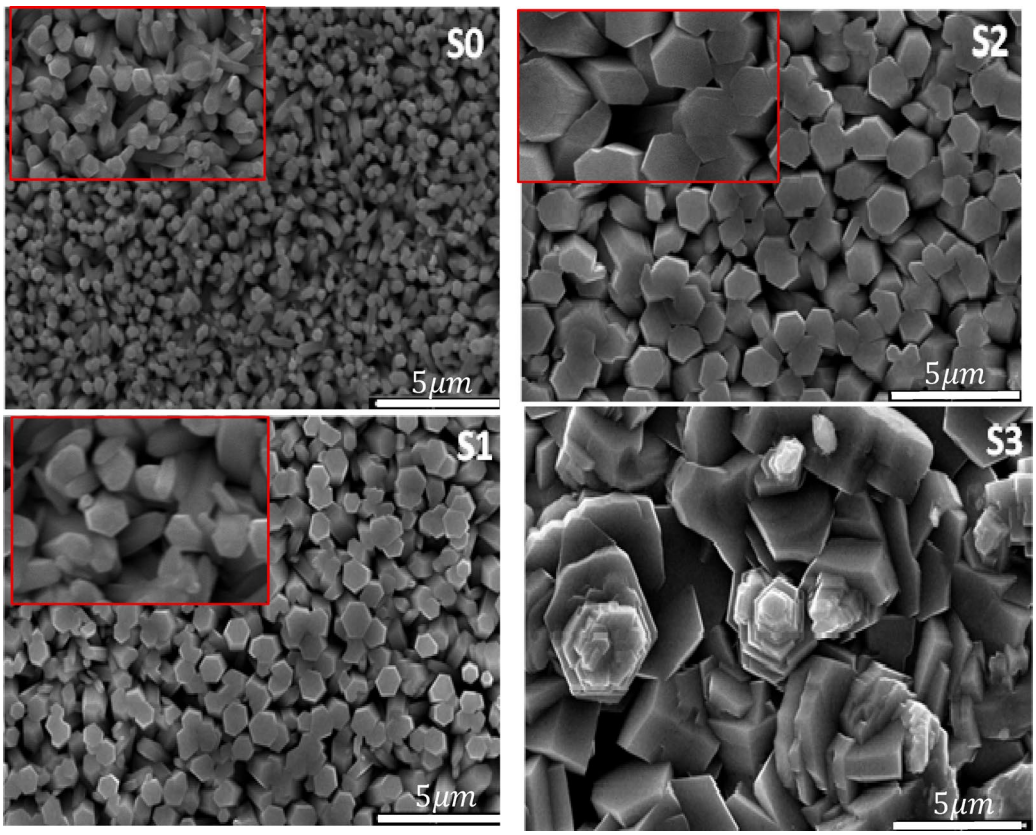

Fig. 1. The SEM images of $Zn_{1-x}Co_xO$ NRs at different concentrations of Co. The inset SEM images show magnified nanorods.

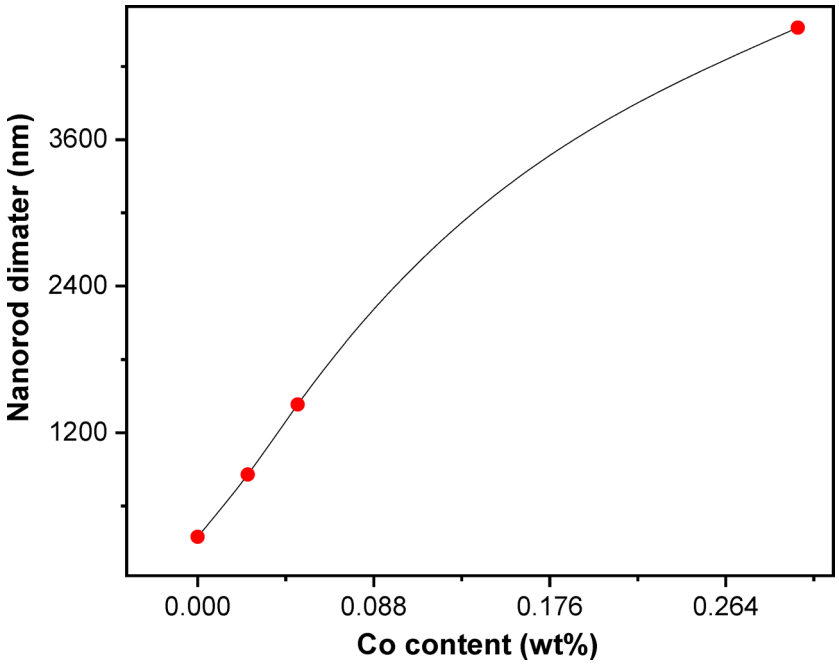

Fig. 2. The nanorod diameter against the Co content. The solid curve represents a non-physical guide for the eye only, connecting discrete data points.

Samples	diameter (nm)	*R*	Wt % Zn	Wt % Co	Wt % O
S0	347	0.98	-----	-----	-----
S1	858	0.89	81.21	0.35	18.54
S2	1432	0.92	79.99	0.39	19.62
S3	4518	0.71	78.60	1.39	20.01

Table 1. Diameter, texture coefficient (R), and weight% (Wt %) of the $Zn_{1-x}Co_xO$ nrs.

of OH^- ions during the growth process. The Zn^{2+} and OH^- ions are produced during the electrochemical deposition process according to the reactions:

$$\begin{aligned} Zn(NO_3)_2 &\rightarrow Zn^{2+} + 2NO_3^- \\ NO_3^- + H_2O + 2e^- &\rightarrow NO_2^- + 2OH^- \\ Zn^{2+} + 2OH^- &\rightarrow Zn(OH)_2 \\ Zn(OH)_2 &\xrightarrow{80^\circ} ZnO + H_2O \end{aligned} \quad (1)$$

When the production rate of OH^- ions is much faster than the diffusion rate of Zn^{2+}[39], the growth of NRs will take place mostly along the longitudinal axis. On the other hand, the growth could occur in both the longitudinal and transversal axes, when the rates of the OH^- generation and Zn^{2+} diffusion are in the same order. The diffusion process of Zn^{2+} ions could be enhanced compared to the OH^- ions generation when Co^{2+} and Zn^{2+} ions exist during the growth process. In this case the growth is more likely along the transvers axis and thus NRs with larger diameter will be produced which depends on the Co content. Furthermore, increasing the diameter leads to the NRs overlapping, and this happens because of the lack of free space in which the rods can grow. In this case parts of the NRs are destroyed as clearly seen for the S3 which showed some defects on the surface of the NRs. In conclusion, based on these results, the doping of ZnO by Co ions could control the diameter and in turn the thickness of the NRs, which might be useful for tuning ZnO properties.

The structure of ZnO NRs produced on ITO substrates is shown in Fig. 3. Many sharp diffraction peaks are observed, which confirm the production of the NRs in ZnO. The identified XRD peaks of fabricated ZnO NRs (PDF number: 01-079-0207) correspond to the hexagonal crystal structure with lattice parameters of a = 3.2568 Å, b = 3.2568 Å, and c = 5.2125 Å. Interestingly, the position of the XRD pattern did not show a significant shift in the peak position towards lower 2θ values with increasing Co content, which means that the lattice parameters *a* and *c* do not vary with increasing Co concentration. In addition, there are no observed peaks matching any

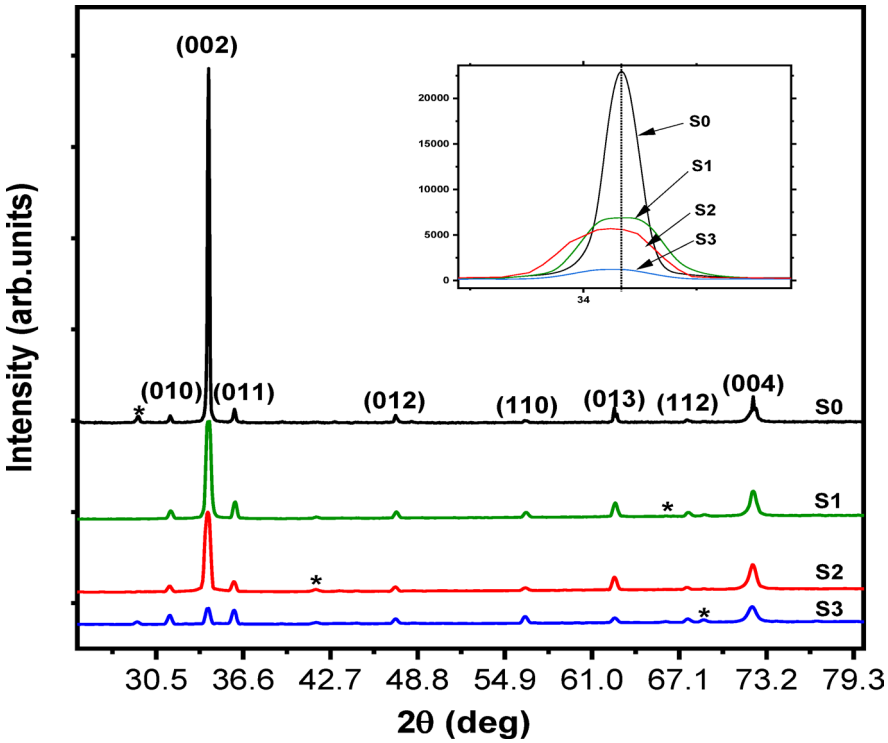

Fig. 3. The XRD pattern of $Zn_{1-x}Co_xO$ NRs at different concentrations of Co. The inset shows the peak (002) on a small scale referring to the change of peak position and intensity with the Co content.

phases associated with the Co except for the peaks labeled (*) that correspond to the ITO substrates. The (002) diffraction peak is the highest intense peak, indicating the great growth along the (002) plane. This result disagrees with those reported[33] where the most intense peak is (101) and reduced by Co addition. Furthermore, as seen in the inset in Fig. 3 the center of the (002) peak is shifted towards lower diffraction angles as well as its intensity is decreased against Co. This indicates the well substitution of Zn^{2+} sites by Co^{2+}. The XRD results are consistent with the observations seen in the SEM images as discussed above.

The XRD was further analyzed to determine the texture coefficient R_{hkl} calculated by[40]:

$$\boldsymbol{R_{hkl}} = \frac{\boldsymbol{I_{hkl}}/\boldsymbol{I_{o(hkl)}}}{1/\boldsymbol{N}\left[\sum_{\boldsymbol{N}} \boldsymbol{I_{hkl}}/\boldsymbol{I_{o(hkl)}}\right]} \tag{2}$$

where I_{hkl} is the recorded XRD intensity of a particular peak has a plane (hkl), $I_{o(hkl)}$ is XRD intensity taken from the reported PDF data. N is the measured peaks. According to the R_{hkl} values (see Fig. 4; Table 1), the growth direction of the $Zn_{1-x}Co_xO$ NRs is found to be along the 002 plane of c-axis. In addition, the decrease of R_{hkl} against Co is due decreasing the (002) peak intensity. The average crystallite size calculated by Scherrer relation ($D = \frac{0.9\lambda}{\beta cos\theta}$)[41] using the three diffraction peaks [(010), (002), (011)] is shown in Fig. 5; Table 2. The Scherer model does not consider the contribution of internal strain, as it fits the peak shape exclusively using a Gaussian function. Figure 5 reveals a clear decrease in crystallite size with increasing cobalt content, dropping from approximately 25.1 nm for the undoped sample (x=0.00) to 25.48 nm at the highest doping level (x = 0.30). This trend suggests that cobalt incorporation effectively suppresses grain growth during material synthesis, likely through a combination of factors: (i) Co segregation creating a solute drag effect that reduces boundary mobility (consistent with Cahn's model of impurity drag, Acta Metall. 1962[42],, and (ii) the nanocrystalline nature of our material where the high density of boundaries amplifies this drag effect (Novikov, Mater. Lett. 2013[43],. Our XRD characterization shows no evidence of secondary phases that could provide Zener pinning, supporting that the stabilization mechanism is primarily kinetic (drag) rather than thermodynamic (pinning), similar to effects reported by Gottstein & Shvindlerman (Grain Boundary Migration in Metals, 2010) for nanoscale systems[44]. Additionally, the addition of Co may result in defects such interstitial cobalt or Ov, which further disturb the crystalline structure and hinder development. To balance growth-inhibiting variables and achieving a minimum achievable crystallite size, the observed plateau at increasing Co concentrations points to a saturation limit for Co substitution within the ZnO lattice.

Additional the Williamson-Hall (W-H) analysis was applied on the samples to determine the crystallite size and strain effects[45]:

$$\beta\cos\theta = \frac{k\lambda}{\boldsymbol{D}} + 4\epsilon\sin\theta \tag{3}$$

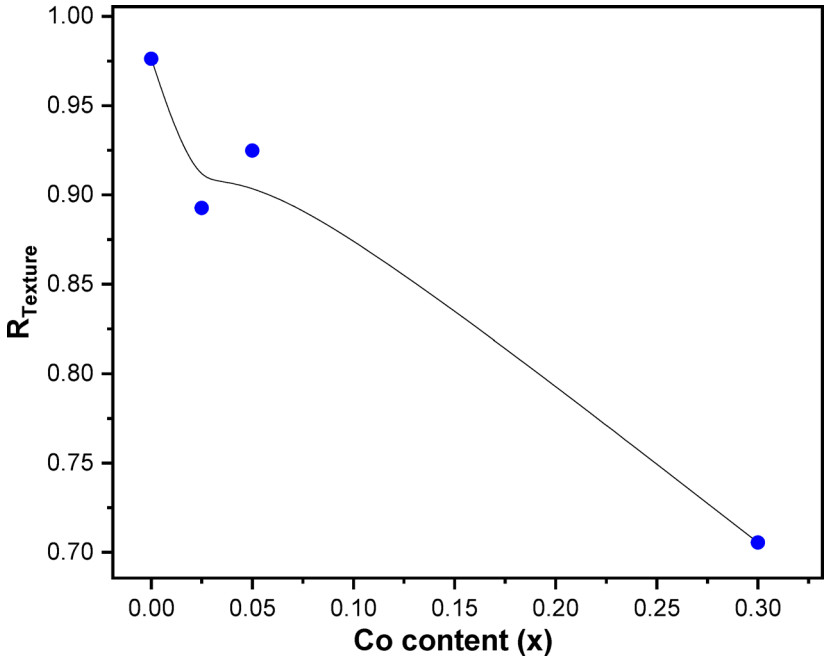

Fig. 4. The texture coefficient versus the Co content of the $Zn_{1-x}Co_xO$ NRs. The solid curve represents a non-physical guide for the eye only, connecting discrete data points.

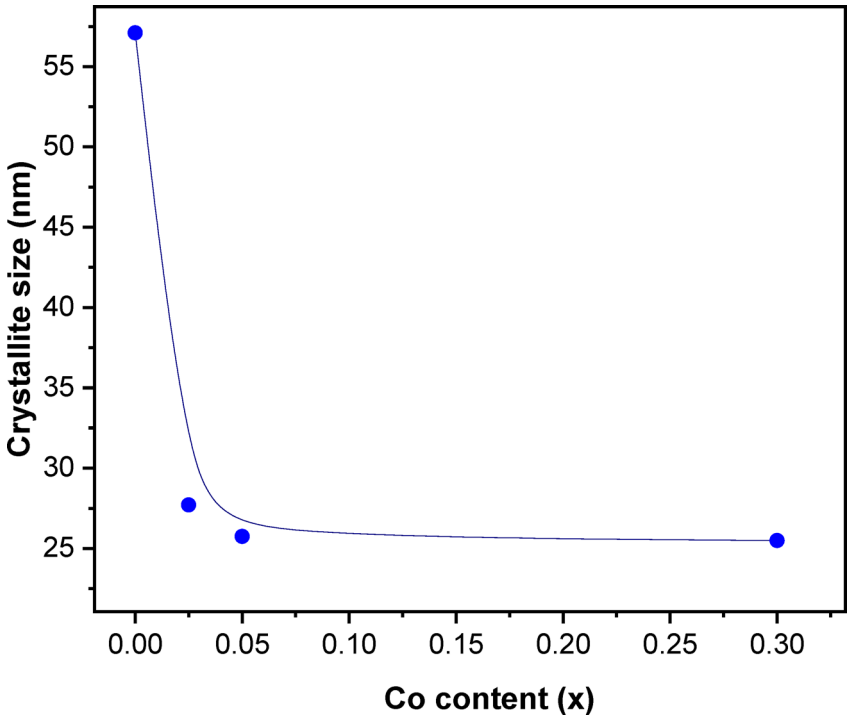

Fig. 5. The crystallite size versus the Co content of the $Zn_{1-x}Co_xO$ NRs. The solid curve represents a non-physical guide for the eye only, connecting discrete data points.

Where β is the FWHM of the XRD diffraction peaks, D is the crystallite size, ϵ is the strain. k = 0.9 and λ is the wavelength of the X-ray radiation. The plot of Eq. 3 is shown in Fig. 6 and the obtained values of crystallite size and strain determined from the intercept and slope of straight lines in Fig. 6, respectively are summarized in Table 2. The good results is obtained for the sample 3, which gave a good fit ($R^2 = 0.87$) showing well-formed nanocrystals about 30 nm in size with very little internal strain. The data of the other samples (S0 and S1) did not show good linear fit.

Samples	XRD Peak	Angle (2 θ)	Scherrer method		Williamson-hall method	
			Crystallite size (D) (nm)	Average crystallite size (nm)	Crystallite size (D) (nm)	Strain
S0	(010)	31.478	48.57	57.10	-	-
	(002)	34.149	73.57			
	(011)	35.963	49.15			
S1	(010)	31.505	27.52	27.70	-	-
	(002)	34.143	24.74			
	(011)	35.994	30.83			
S2	(010)	31.419	28.47	25.75	66.3	0.00289
	(002)	34.077	21.81			
	(011)	35.920	26.95			
S3	(010)	31.430	25.80	25.48	30.1	0.000713
	(002)	34.095	25.34			
	(011)	35.922	25.31			

Table 2. Crystallite size values determined by scherrer and Williamson-Hall method for the $Zn_{1-x}Co_xO$ nrs.

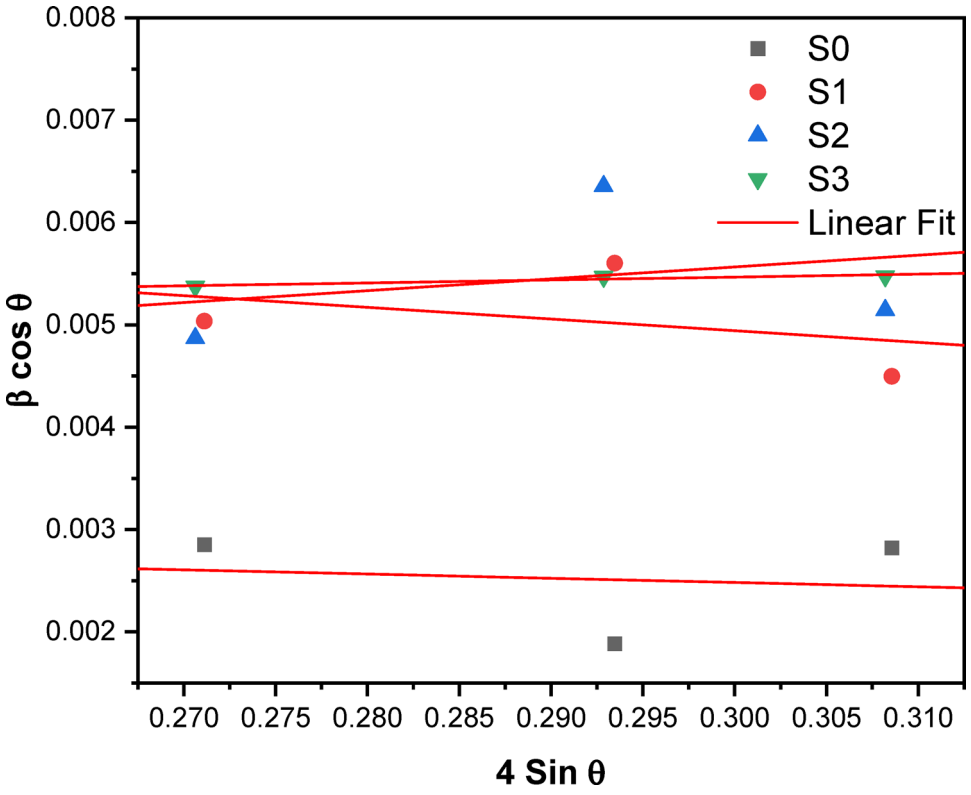

Fig. 6. The relation between $\beta\, cos\theta$ and $4sin\theta$ [Williamson-Hall plot] of $Zn_{1-x}Co_xO$ NRs.

The EDX spectra of $Zn_{1-x}Co_xO$ NRs, shown in Fig. 7, confirms the presence of host elements Zn and O as well as the dopant Co with different weight and atomic percentages in the fabricated NRs. It is noticed that the prepared Co-doped ZnO NRs are pure and free from impurities, which favor the doping of Co into the ZnO lattice. Although compositional of EDX analysis is inconsistent with the starting compositions, the wt% of Co increases, whereas the wt% of Zn decreases. It was further found that the wt % and at % of O increase with increasing Co level which indicates that the Ov defects reduced with the increment of the Co, which may affect the structural properties. However, the values of wt% are listed in Table 1.

Optical properties

The optical absorbance (A) and absorption coefficient (α) of $Zn_{1-x}Co_xO$ NRs samples are shown in Fig. 8. The values of α are determined using: $\alpha = \frac{2.302}{d}A$, where d is the layer thickness. It is seen that both A and α are increased as one go toward the short UV wavelength (λ). This behavior is attributed to the e-h pair formation when the hν is in the order of the E_g. They are also increased against Co content, which could be attributed to

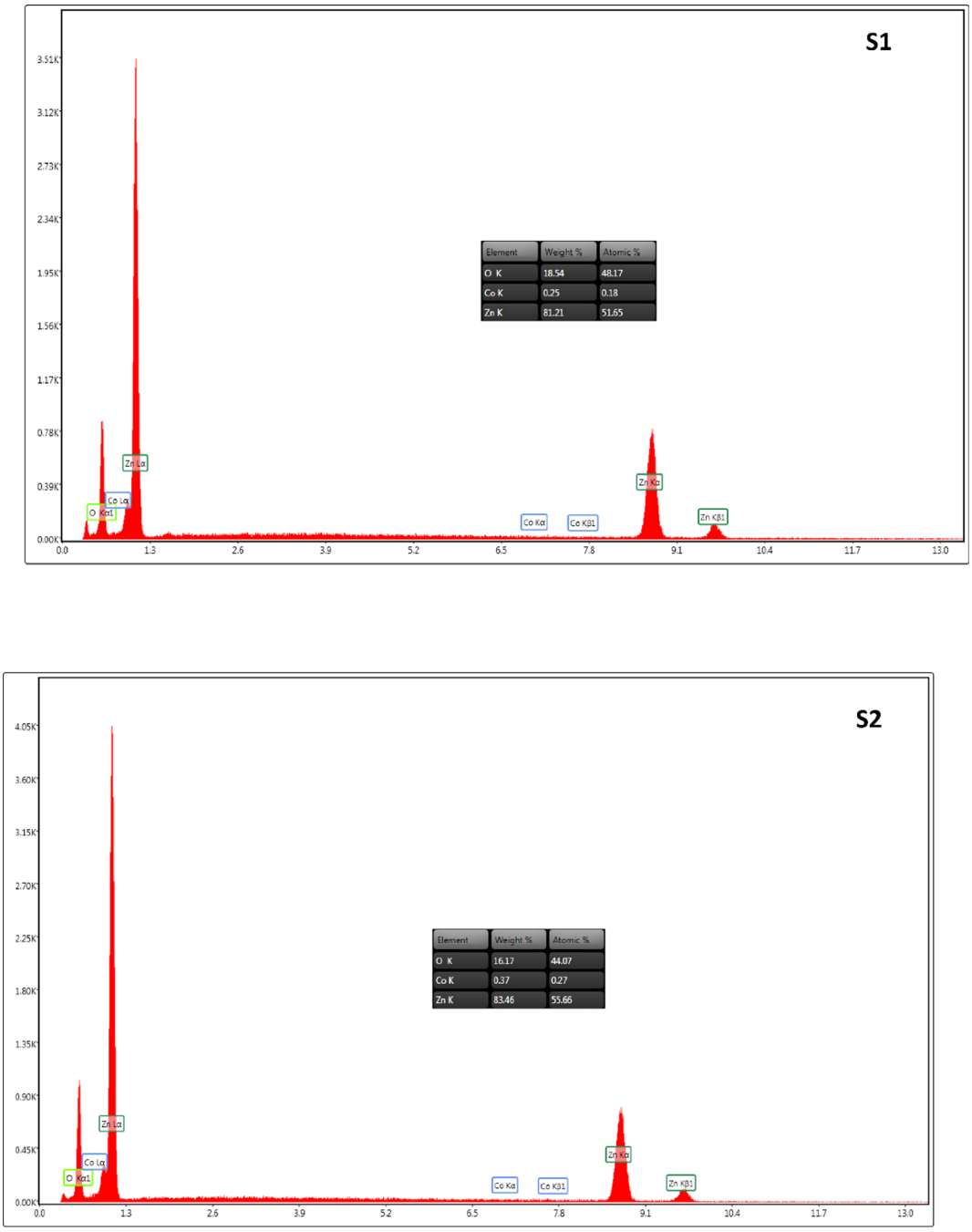

Fig. 7. The EDX spectra of $Zn_{1-x}Co_xO$ NRs.

increasing the size of the NRs as observed in the SEM images. The band gap of $Zn_{1-x}Co_xO$ NRs samples was obtained using the linear plot between $(\alpha h\nu)^2$ and hv, shown in Fig. 9 using the Tauc formula for the direct transition[36,37]. This plot behavior indicated that all NRs samples have only one fundamental absorption edge, one E_g value.

Figure 10 plots the bandgap energy (E_g) of the nanorods as a function of Co concentration. It is seen that E_g is 3.32 ± 0.04 eV for undoped ZnO NRs, but it reduced to 3.24 ± 0.04 eV for the doped sample S3. The E_g of the doped and undoped ZnO NRs are comparable with those reported in the literature[46,47]. Reducing the E_g of ZnO NRs by Co can be attributed to increasing the diameter of the NRs. In addition, Co incorporation into the ZnO lattice introduces additional energy states within the band gap. This mechanism can cause band tailing, where the edges of the conduction and valence bands extend into the E_g region, thus reducing the E_g. The observed tuning of the band gap (E_g) with the incorporation of Co ions suggests a mutual interaction between the doped Co ions and the band structure of the ZnO nanorods host lattice. The observed reduction in the E_g with increasing Co content may be related to the expected structural phase of ZnCoO that has a lower optical E_g. Hence, the depletion potential in the Co-doped ZnO was foreseen to have a band structure with lower E_g

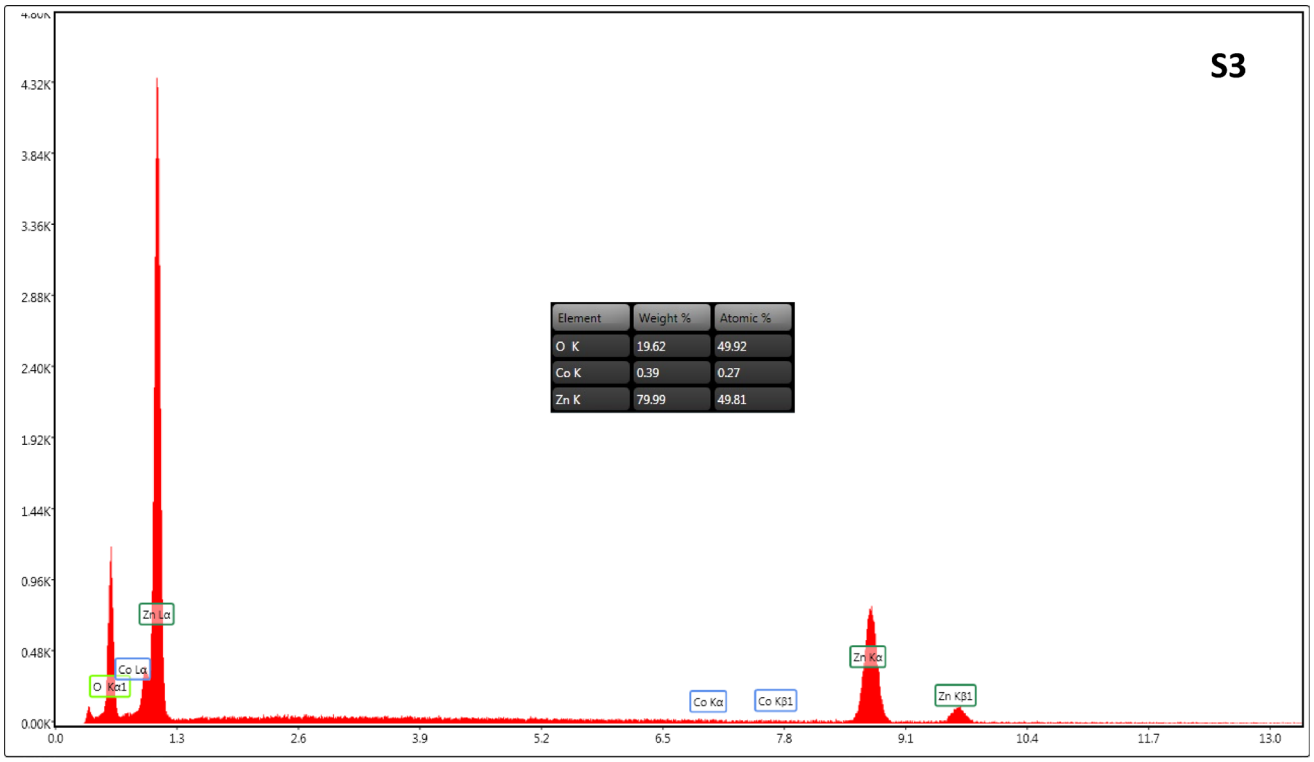

Fig. 7. (continued)

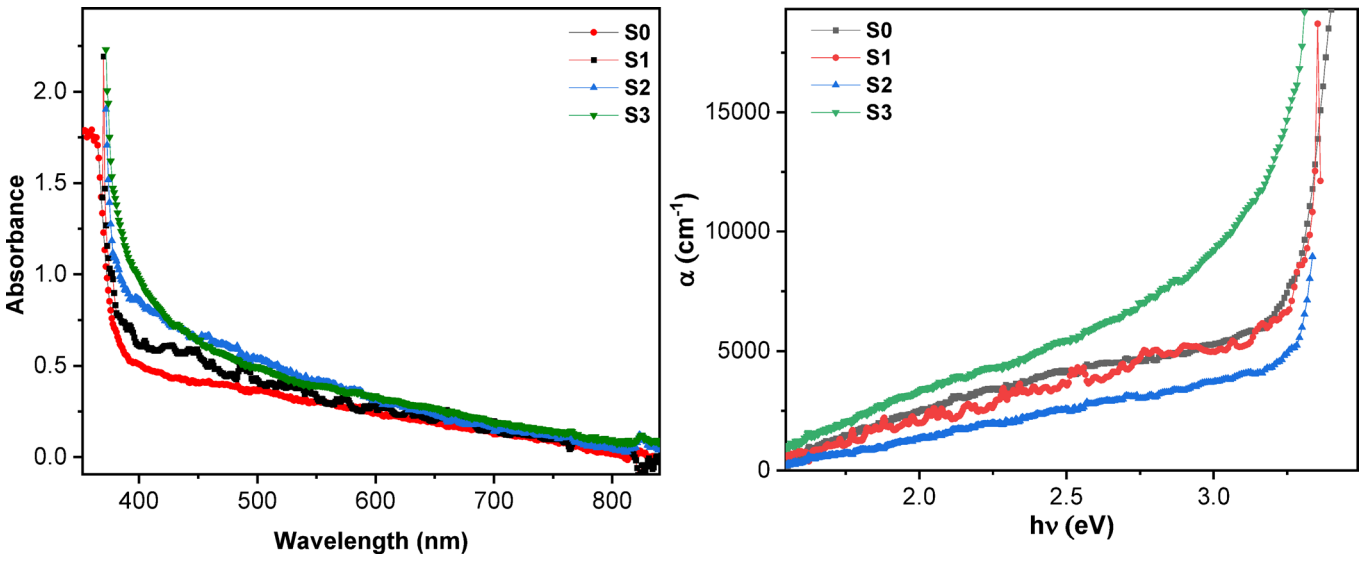

Fig. 8. The optical absorbance and absorption coefficient of $Zn_{1-x}Co_xO$ NRs at different concentrations of Co.

compared with the as-synthesized ZnO NRs. Moreover, the reduction in the bandgap may be attributed to the sp-d exchange interactions between the band electrons in ZnO and the localized d-electrons of the Co^{2+} ions[48]. Such interaction influences the electronic structure of ZnO. These interactions can modify the band edge positions, leading to E_g narrowing. Thus, our electrochemical synthesis achieves precise bandgap tuning in $Zn_{1-x}Co_xO$ nanorods, reducing E_g from 3.32 eV (undoped) to 3.24 eV (x = 0.30). This 0.08 eV shift, though smaller than the 0.34 eV reduction reported by Basith et al. for microwave-synthesized nanoparticles (from 3.22 eV to 2.88 eV at x = 0.20), demonstrates superior linearity and stoichiometric control. The difference arises from our lower doping range ($\leq$ 0.30 wt% vs. 0–2 wt%) and distinct defect chemistry. This controlled bandgap narrowing, coupled with hexagonal NRs morphology, better suits wavelength-specific optoelectronic devices like UV photodetector[46,47,49,50].

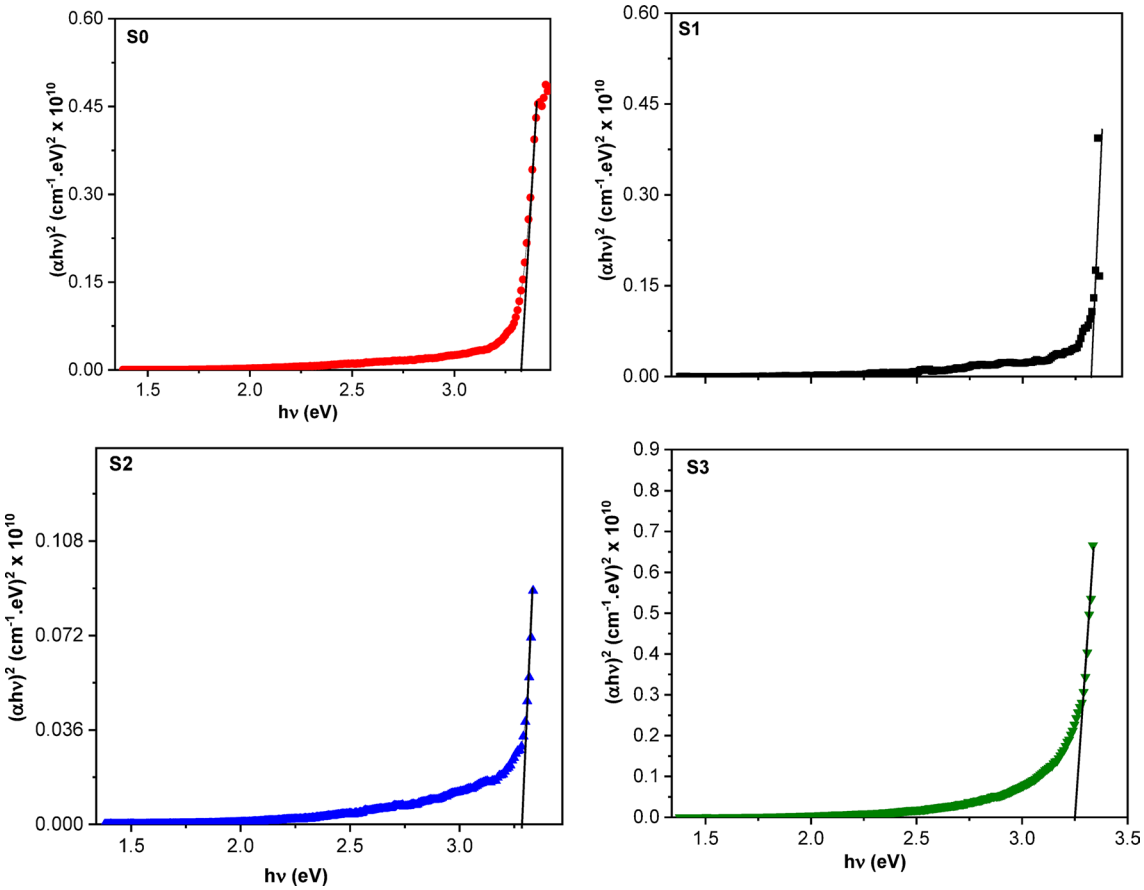

Fig. 9. The Tauc plots of $Zn_{1-x}Co_xO$ NRs at different concentrations of Co.

Magnetic properties

Figure 11 demonstrates the measured magnetization as a function of the applied magnetic field (M-H curves) at temperatures (T) of 300 and 10 K, respectively. At 300 K, the behavior of So and S1 is diamagnetic with magnetizations at 20,000 Oe of 0.016 and 0.011 emu/g, respectively. With more increase of Co up to 0.05%, the behavior became weekly ferromagnetic of 0.016 emu/g in the low field region (0-2000 Oe), and diamagnetic of 0.055 emu/g in the high field region (2000–20000 Oe). This result agrees with those reported for ZnO NRs of 36 nm diameter, which reveal the double behaviors of ferromagnetic and diamagnetic[8,38,39]. This behavior may be related to the interfacial defects in the NRs which were beneficial for various types of magnetization. The observed dependence of magnetic behavior on the field demonstrated that the defect states between ZnO and CoO interfaces would be in a metastable state, where the spatial distribution strongly depends on the strength of the field[51].

Interestingly, the S3 exhibits unusually strong ferromagnetic behavior of 0.14 emu/g and a considerable hysteresis loop. However, with decreasing temperature to 10 K, all NRs samples show paramagnetic behaviors In addition, the M-H curve deviates slightly from its Linearity in the low field region below 2000 Oe. Further, such deviation was increased with increasing the Co content, which may be due to increasing the growth of the magnetic anisotropy plane in the ZnO NRs host lattice[52,53]. The strong paramagnetic behavior of small hysteresis area shown for S3 at 10 K is, of course, good evidence for residual ferromagnetic domains generated with decreasing the temperature and increasing Co. However, it has been reported that decreasing the Ov to a critical value can degrade the ferromagnetic ordering, leading to a reduction in ferromagnetism[54–56]. It is expected the super-exchange paramagnetic centers of S3 were substituting for the ferromagnetic exchange through F-centers as the temperature dropped to 10 K.

The measured magnetization curves indicate the co-existence of two components: paramagnetic and ferromagnetic at 10 K and diamagnetic and ferromagnetic at 300 K. The paramagnetic and diamagnteic contributions (i.e. the linear part) at high magnetic field values were subtracted to extract the ferromagnetic properties. The residual portion of the ferromagnetic is then plotted in Fig. 12. It is seen that all NR samples reveal the hysteresis loop at both considered temperatures. The loop is dependent on the chosen Co and temperature, since it increases with increasing the Co content. However, the magnetic parameters, including the saturated and remnant magnetizations M_s and M_r and the coercive field H_c, are listed in Table 3. The values of M_s and M_r are slightly increased by reducing the T from 300 to 10 K and also by increasing the Co content as well. Interestingly, the sample S2 showed the highest value for H_c of 128.36 and 332.81 Oe compared to the other NR, indicating that S2 is a hard type of material. Although the S3 is the soft NRs sample among the others (with H_c = 16–27 Oe),

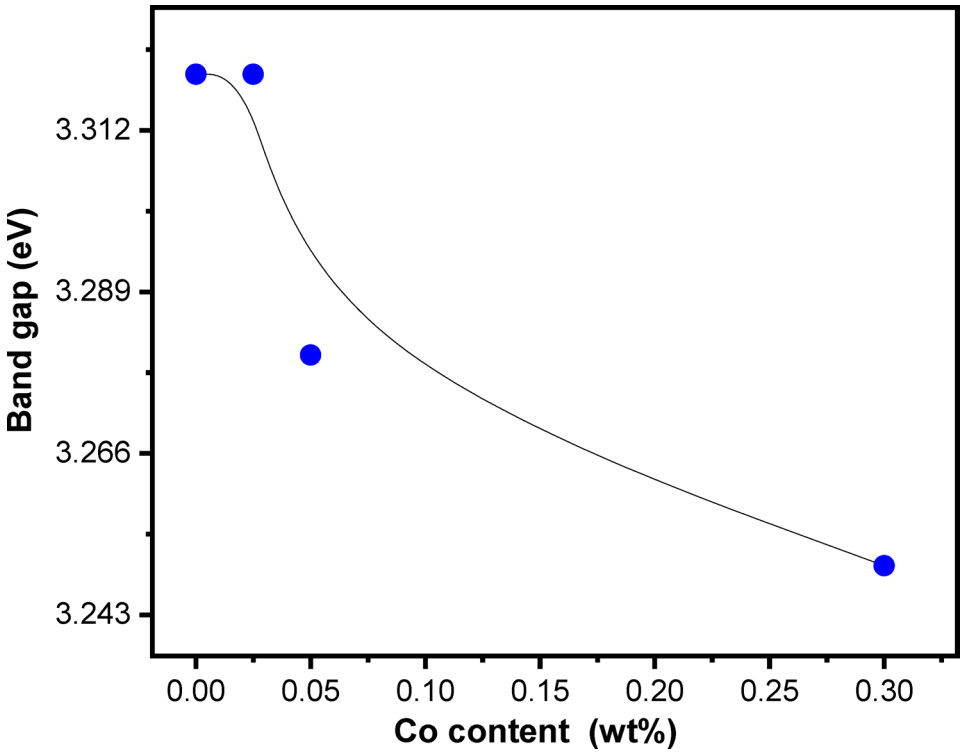

Fig. 10. The band gap of $Zn_{1-x}Co_xO$ NRs against the Co content. The solid curve represents a non-physical guide for the eye only, connecting discrete data points.

it exhibits strong ferromagnetism with M_s (= 0.14 and 0.18 emu/g) and high M_r (0.022 and 0.035 emu/g) at 10 K and 300 K, respectively. Although the behavior of M_s against Co doping agrees with that reported elsewhere, the current values of M_s are higher than those reported in[9,25,40], which highlights the present investigation. While Basith et al. report weak RTFM ($M_s = 2.2 \times 10^{-3}$ emu/g at 2 wt%), our nanorods exhibit significantly stronger ferromagnetism (M_s = 0.14 emu/g at 0.30 wt%). This enhancement stems from shape anisotropy of NRs promoting spin alignment and optimized oxygen mediation (evidenced by rising O content with Co doping). Notably, our coercivity range (16-332.81Oe) spans both soft (memory) and hard (sensor) magnetic regimes, a feature absent in their nanoparticle system. The combination of higher M_s and tunable Hc positions our NRs as superior candidates for spin-based devices.

On the other hand, variations in magnetic moment μ (μ_B) = (WM_s/5585), squareness Sq = (M_r/M_s), and magnetic anisotropy γ = (H_cM_s/0.98)[38,57,58] are summarized in Table 3. It is evident that the S3 NRs exhibit higher values for Sq and μ as well as obtained for the M_s, whereas the value of γ is the bigger for the S2. These findings indicted that Sq and μ are controlled by M_s, whereas γ is controlled by H_c. Furthermore, Sq is less than 0.50 for all NRs, indicating magneto-static interaction for all NRs[59,60]. Therefore, S3 is of particular interest here for the design of ZnO spintronic devices.

The FC and ZFC curves shown in Fig. 13 show that there is no obvious bifurcation with blocking temperature in the whole temperature range of 10–300 K, suggesting that there are no ferromagnetic nanoclusters. In addition, the magnetization increases with the content of cobalt which reveals that the Curie temperature (T_C) is higher than 300 K and supporting the co-existing of monetization behavior with pragmatic behavior at low temperature and diamagnetic behavior at high temperate. However, this result shows bifurcation in the ZFC/FC curves increases with increasing Co content, as indicating that the level of nonmagnetic nano-grains increases with the Co content with weak antiferromagnetic contribution.

The magnetic properties of pure ZnO nanorods might be due to the formation of Ov[8,61]. However, the origin of the ferromagnetization for Co doped ZnO NRs could be attributed to the following reasons: The interaction between the Co ions and the host ZnO lattice which is usually linked to the origin of magnetization in the doped samples. In addition, Co doping ZnO allows the Co^{2+} ions to take the place of Zn^{2+} ions in the ZnO lattice. The unpaired d electrons in the Co^{2+} ions can engage in exchange interactions with one another. Depending on the exchange interaction's nature and the distance between the Co ions, these interactions can result in either antiferromagnetic or ferromagnetic ordering. In certain instances, charge carriers (electrons or holes) can facilitate magnetic interactions between Co ions, a phenomenon known as carrier-mediated ferromagnetism. These carriers can amplify the interaction between localized magnetic moments on the Co ions, resulting in long-range magnetic ordering.

Co exhibited an interesting feature that opened the way to controlling the RTFM through either tuning the interfacial defect states or inducing a localized spin of doped transition metal ions. It is believed that a tendency to form the Zn-O-Co ferromagnetic cluster is strongly related to the size and distribution of the Ov

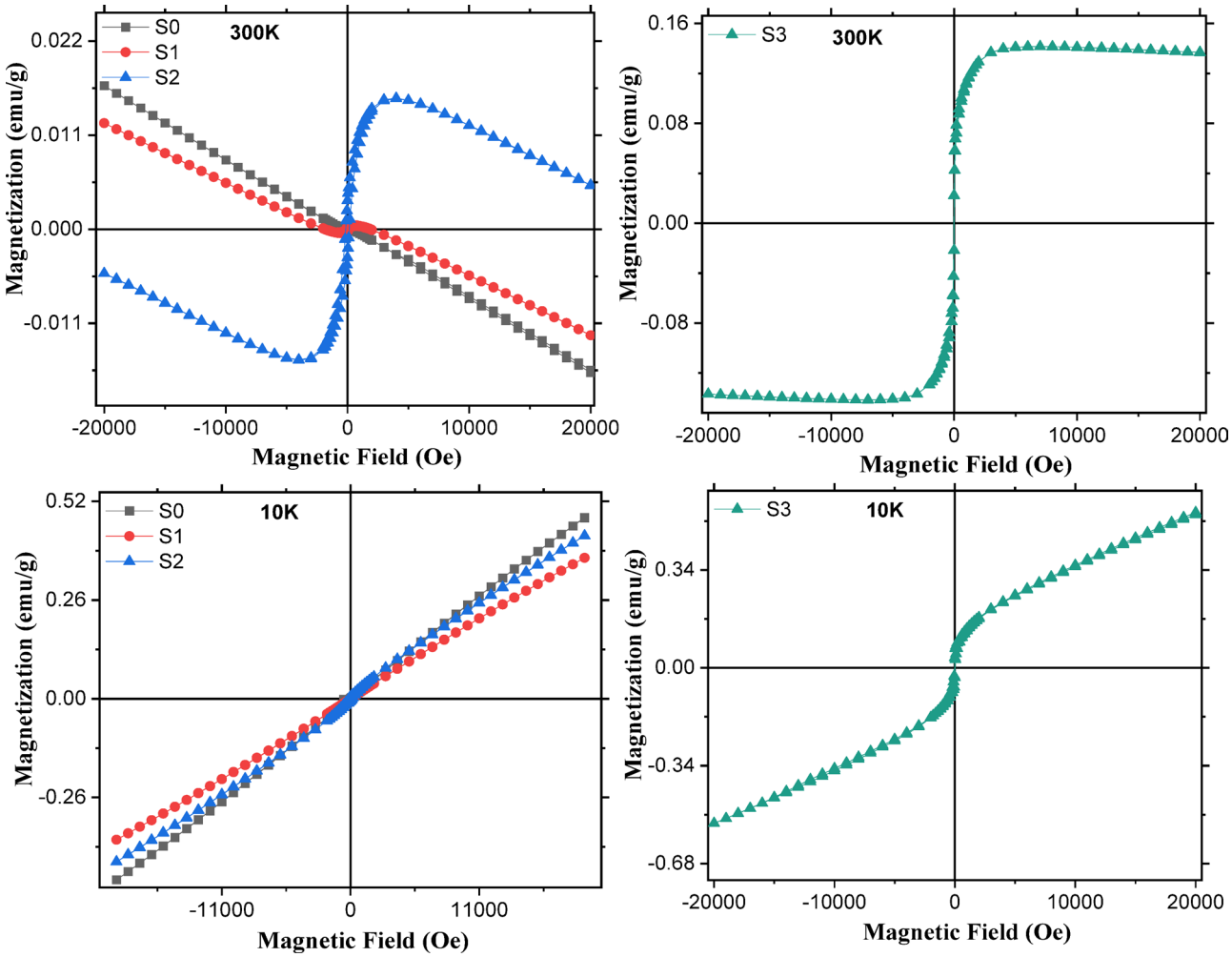

Fig. 11. The magnetization dependence of the magnetic field of $Zn_{1-x}Co_xO$ NRs at different concentrations of Co. (Top): raw data measured at 10 K and (bottom): raw data measured at 300 K.

defect states, where the double-exchange interaction governs the behavior RTFM[62]. The RTFM for S3 even at RT was ascribed to the combined effect of the interaction of localized spin around the incorporated Co-ions at the tetrahedral sites with accumulated charge carriers of ZnO to form bound magnetic polarons[63]. Anyhow, the coexistence of different magnetic behaviors in Co-doped ZnO has been reported[64]. They found that Ov plays an important mediation role in Co-Co ferromagnetic coupling rather than a Co ferromagnetic moment and induced ferromagnetic domains at higher Co level. It has been also reported that the presence of grouped Co^{2+} ions, revealing the presence of clusters of high spin Co^{2+} with antiferromagnetically coupled spins, besides the ferromagnetic[36]. Thus, the schematic in Fig. 14 demonstrates the evolution of magnetic behavior in Co-doped ZnO across doping levels and temperatures. In undoped ZnO, oxygen vacancies (Ov) introduce localized paramagnetic spins (↑), though bulk diamagnetism dominates. At low Co doping (0.025–0.05%), bound magnetic polaron (BMP) form via electron hopping between Co^{2+} ions through Ov, creating isolated ferromagnetic (FM) clusters amid diamagnetic regions. For high Co (0.30%), dense Co^{2+} clusters and Ov channels drive long-range FM, evidenced by enhanced magnetization and hysteresis. At 10 K, thermal energy suppression randomizes spins (↑↓), leading to paramagnetism.

Conclusion

The structural, optical, and magnetic properties of $Zn_{1-x}Co_xO$ nanorods (NRs) fabricated by electrochemical deposition have been investigated. All NR samples were grown along the (002) plane and have a hexagonal structure. The doping of ZnO with Co up to 0.30 wt% could decrease the crystallite size and the texture coefficient of ZnO NRs, whereas the NRs diameter was increased. Interestingly, the Co doping could induce more Ov through the lattice of ZnO NRs. The E_g was found to be 3.32 eV for the ZnO NRs and then reduced to 2.24 eV at the highest level of Co content. At 300 K, the magnetic behavior of both of So and S1 is diamagnetic, weakly ferromagnetic, and diamagnetic for S2, and strong ferromagnetic for S3. But all NRs samples show paramagnetic behaviors with higher magnetization at 20 kOe as the temperature decreases to 10 K. In addition, the S2 showed the highest value for coercive field as compared to the other NRs, indicating hard type material. The S3 exhibited

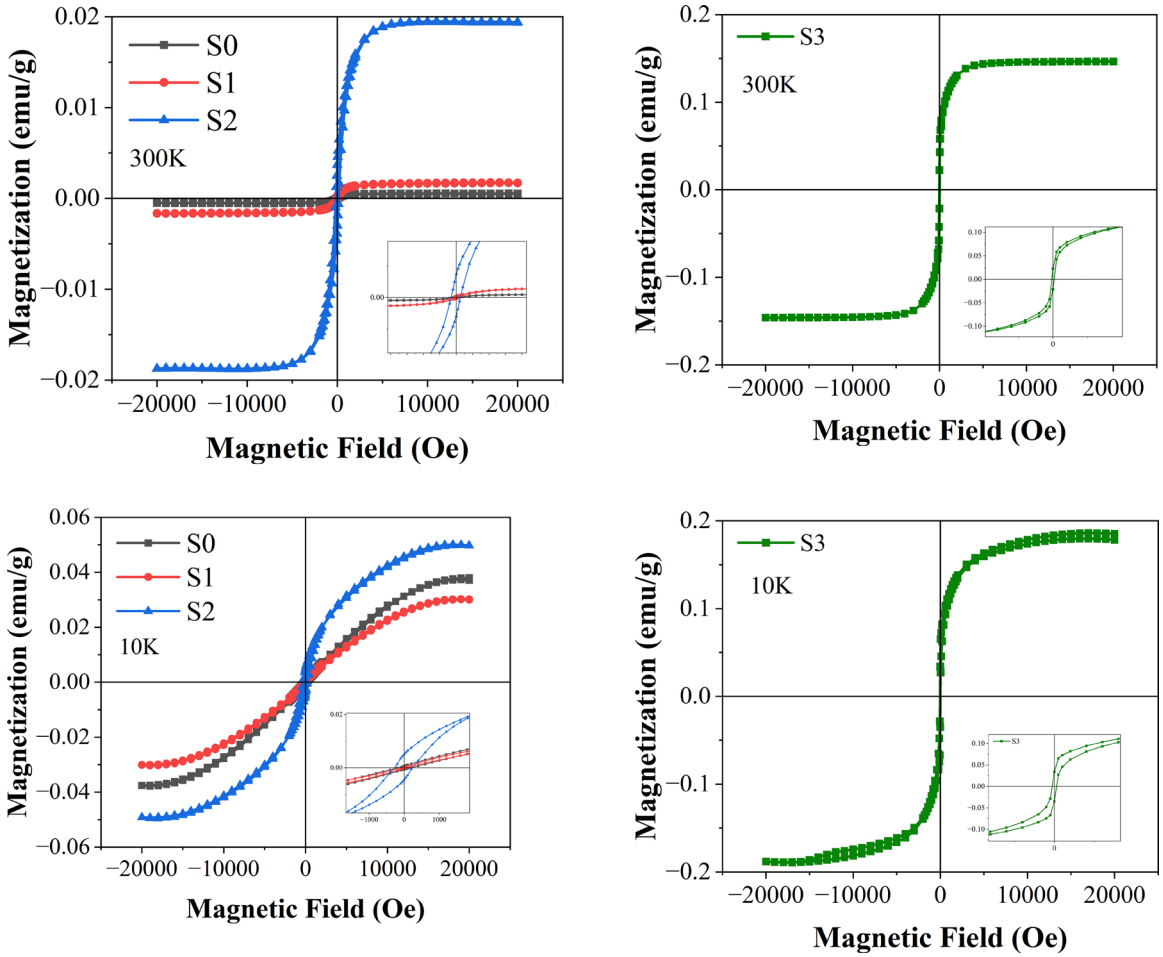

Fig. 12. The magnetization dependence of the magnetic field of $Zn_{1-x}Co_xO$ NRs (Top): corrected data measured at 300 K and (bottom): corrected data measured at 10 K.

Samples	M_s (emu/g) 300 K	M_s (emu/g) 10 K	M_r (emu/g) 300 K	M_r (emu/g) 10 K	H_c (Oe) 300 K	H_c (Oe) 10 K
S0	0.0005	0.038	0.0000439	0.000767	58.85	208.24
S1	0.0017	0.030	0.000257	0.000266	64.78	52.23
S2	0.0190	0.050	0.0037	0.0052	128.36	232.81
S3	0.1400	0.180	0.022	0.035	16.57	27.92
	Sq 300 K	**Sq 10 K**	**γ (emu. Oe/g) 300 K**	**γ (emu. Oe/g) 10 K**	**μ (μ_B) x10^{-5} 300 K**	**μ (μ_B) x10^{-5} 10 K**
S0	0.0878	0.0202	0.0300	8.076	0.729	5.54
S1	0.1512	0.0089	0.1124	1.599	2.47	43.6
S2	0.1947	0.1040	2.489	11.878	27.6	72.6
S3	0.1571	0.1944	2.367	5.129	199	256

Table 3. The corrected magnetic parameters of $Zn_{1-x}Co_xO$ NRs at different concentrations of Co.

strong ferromagnetism with the highest values of M_s. For S0, the magnetizations of Fc and ZFC curves are typically the same over the full temperature range. Such behavior could be only obtained at 200 K, 265 and 300 K for the other NRs, respectively. The magnetizations at 300 K are gradually increased with increasing the Co content. These findings suggest the $Zn_{1-x}Co_xO$ NRs could be valuable for both optoelectronic and spintronic devices. The ability to control both optical and magnetic properties through simple electrochemical growth is especially promising. It has been shown that by carefully tuning the electrochemical process, nanorods with specific combinations of optical and magnetic behavior can be produced- something that could be really valuable

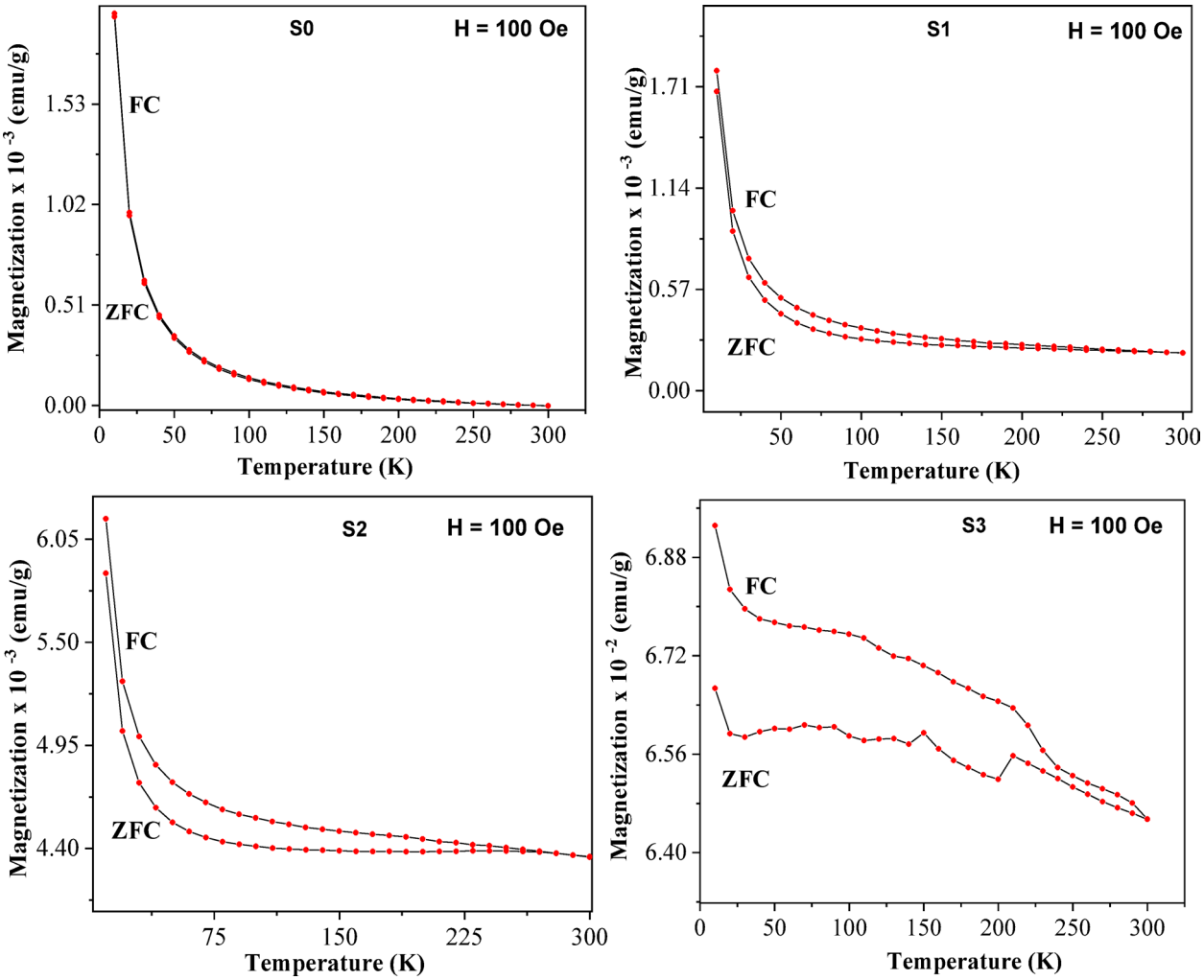

Fig. 13. The magnetization dependance of temperature of $Zn_{1-x}Co_xO$ NRs at different concentrations of Co.

for developing new types of devices that need to work in challenging environments like space or nuclear facilities. There's still more to explore, particularly in how these materials perform under actual radiation exposure, but these results open some exciting possibilities for future research and applications.

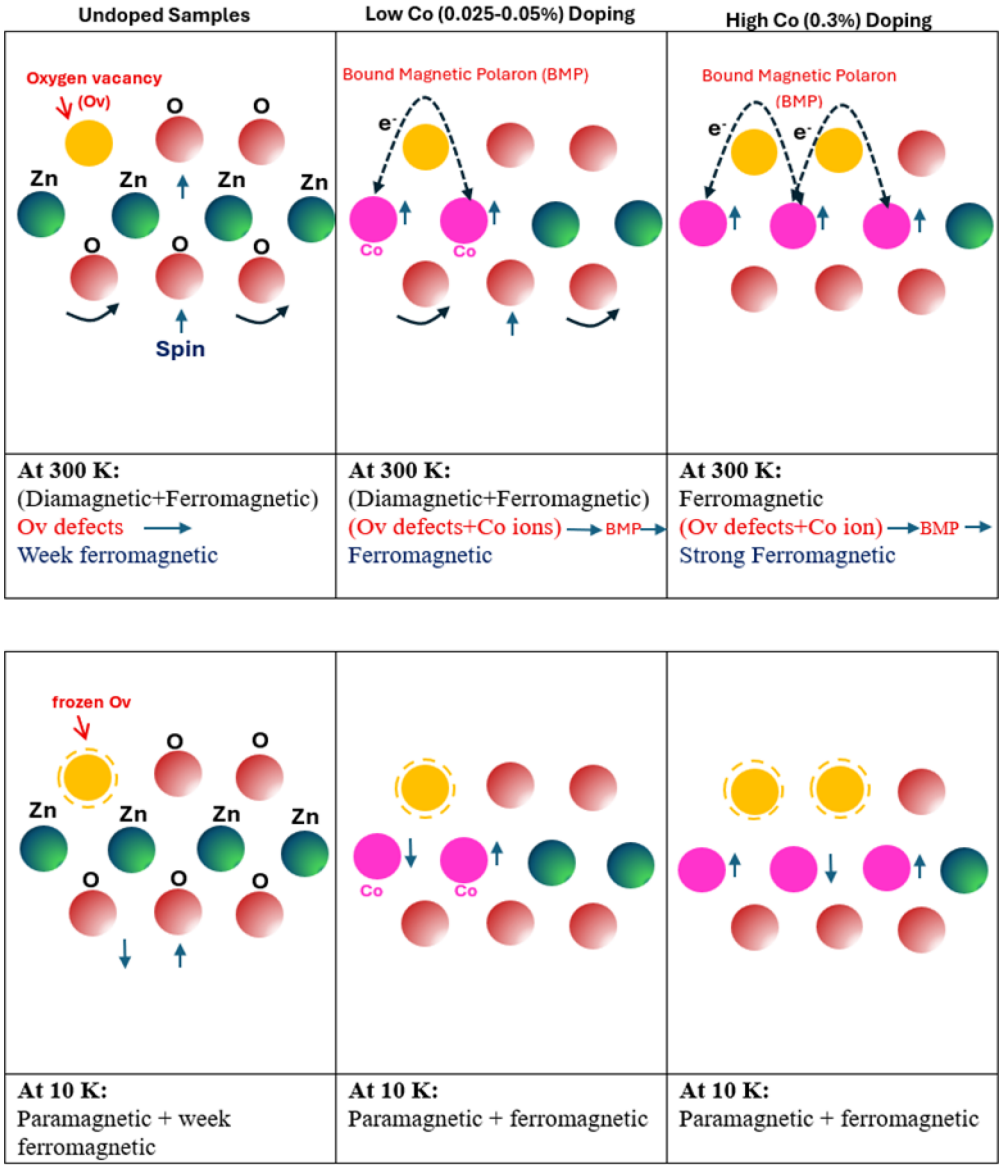

Fig. 14. A schematic diagram demonstrating the magnetization at 300 K and 10 K of $Zn_{1-x}Co_xO$ NRs at different concentrations of Co.

Data availability

The data generated and/or analyzed during the present study are avaliable in: https://doi.org 10/5281/zenodo.15466514.

Received: 6 May 2025; Accepted: 10 September 2025
Published online: 30 October 2025

References

1. Techalertmanee, T. et al. Facile synthesis of zinc-iron mixed oxide/carbon nanocomposites as nanocatalysts for the degradation of methylene blue. *Mater. Lett.* **145**, 224–228. https://doi.org/10.1016/j.matlet.2015.01.079 (2015).
2. Sharma, D. K., Shukla, S., Sharma, K. K. & Kumar, V. A review on ZnO: Fundamental properties and applications, Mater. Today Proc. https://doi.org/https://doi.org/ (2020). https://doi.org/10.1016/j.matpr.2020.10.238
3. Kumar, S. Exploration of structural, morphological and magnetic properties of transition metal doped SnO2 films grown using pulsed laser deposition. *Vacuum* **182** https://doi.org/10.1016/j.vacuum.2020.109725 (2020).
4. Xing, G. et al. Correlated d0 ferromagnetism and photoluminescence in undoped ZnO nanowires. *Appl. Phys. Lett.* **96** https://doi.org/10.1063/1.3340930 (2010).
5. Hong, N. H., Sakai, J., Huong, N. T., Poirot, N. & Ruyter, A. Role of defects in tuning ferromagnetism in diluted magnetic oxide thin films. *Phys. Rev. B - Condens. Matter Mater. Phys.* **72** https://doi.org/10.1103/PhysRevB.72.045336 (2005).
6. Satpathy, S. K. et al. Structural, optical, antimicrobial and ferromagnetic properties of Zn1 – xLaxO nanorods synthesized by chemical route. *J. Alloys Compd.* **865** https://doi.org/10.1016/j.jallcom.2021.158937 (2021).

7. Sedky, A., Amin, S. A. & Mohamed, M. Electrical, photoluminescence and ferromagnetic characterization of pure and doped ZnO nanostructures. *Appl. Phys. Mater. Sci. Process.* **125** https://doi.org/10.1007/s00339-019-2612-y (2019).
8. Shoushtari, M. Z., Poormoghadam, A. & Farbod, M. The size dependence of the magnetic properties of ZnO and Zn 1-x Ni x O nanoparticles. *Mater. Res. Bull.* **88**, 315–319. https://doi.org/10.1016/j.materresbull.2017.01.006 (2017).
9. Wu, X. et al. Optical and magnetic properties of Fe doped ZnO nanoparticles obtained by hydrothermal synthesis, **2014** 1–6. (2014). https://doi.org/10.1155/2014/792102
10. Sedky, A., Afify, N., Almohammedi, A., Ibrahim, E. M. M. & Ali, A. M. Structural, optical, photoluminescence and magnetic investigation of doped and Co-doped ZnO nanoparticles. *Opt. Quantum Electron.* **55** https://doi.org/10.1007/s11082-023-04718-8 (2023).
11. Sedky, A. & El-Suheel, E. A comparative study between the effects of magnetic and nonmagnetic dopants on the properties of ZnO varistors. *Phys. Res. Int.* **2010** https://doi.org/10.1155/2010/120672 (2010).
12. Chanda, A., Gupta, S. & Vasundhara, M. Study of structural, optical and magnetic properties. *RSC Adv.* **7**, 50527–50536. https://doi.org/10.1039/C7RA08458G (2017).
13. Xia, B. Y. et al. One-dimensional nanostructures: synthesis, characterization, and applications. *Adv. Mater.* **15**, 353–389 (2003).
14. Kuchibhatla, S. V. N. T., Karakoti, A. S., Bera, D. & Seal, S. One dimensional nanostructured materials. *Prog Mater. Sci.* **52**, 699–913. https://doi.org/10.1016/j.pmatsci.2006.08.001 (2007).
15. Panigrahy, B. B., Aslam, M., Misra, D. S., Ghosh, M. & Bahadur, D. Defect-related emissions and magnetization properties of ZnO nanorods, 1161–1165. (2010). https://doi.org/10.1002/adfm.200902018
16. Guo, B. et al. Comparative study of room-temperature ferromagnetism in cu-doped ZnO nanowires enhanced by structural inhomogeneity **, 3521–3527. (2008). https://doi.org/10.1002/adma.200703149
17. Panda, J., Sasmal, I. & Nath, T. K. Magnetic and optical properties of Mn-doped ZnO vertically aligned nanorods synthesized by hydrothermal technique. *AIP Adv.* **6** https://doi.org/10.1063/1.4944837 (2016).
18. Singh, J. & Singh, R. C. Tuning of structural, optical, dielectric and transport properties of Fe-doped zno:v system. *Mater. Sci. Semicond. Process.* **121** https://doi.org/10.1016/j.mssp.2020.105305 (2021).
19. Wu, Z. F. et al. Effect of al co-doping on the electrical and magnetic properties of Cu-doped ZnO nanorods, **615** 521–525. (2014). https://doi.org/10.1016/j.jallcom.2014.06.204
20. Zhang, T. et al. Applied catalysis B: environmental Co @ C nanorods as both magnetic stirring nanobars and magnetic recyclable nanocatalysts for microcatalytic reactions. *Appl. Catal. B Environ.* **304**, 120925. https://doi.org/10.1016/j.apcatb.2021.120925 (2022).
21. Wang, W., Han, Q., Tang, L., Tian, J. & Kang, C. Microstructure-dependent magnetic anisotropy in Nanorod vanadium oxide room-temperature ferromagnetic thin films using reactive sputtering. *Thin Solid Films*. **780**, 139964. https://doi.org/10.1016/j.tsf.2023.139964 (2023).
22. Meng, J. Various electromagnetic properties of magnetic Fe-based nanorods in ghz range. *J. Alloys Compd.* **960**, 170805. https://doi.org/10.1016/j.jallcom.2023.170805 (2023).
23. Narasimman, S., Balakrishnan, L. & Alex, Z. C. Materials science in semiconductor processing highly sensitive magnetic field sensor based on uniform core fiber using Mn doped ZnO nanorods as cladding. *Mater. Sci. Semicond. Process.* **166**, 107732. https://doi.org/10.1016/j.mssp.2023.107732 (2023).
24. IglesiasG.R. Solvothermally synthesized magnetite nanorods for application in magnetic hyperthermia and photothermia. *J. Magn. Magn. Mater.* **596** https://doi.org/10.1016/j.jmmm.2024.171990 (2024).
25. Tun Naziba, A. et al. Structural, optical, and magnetic properties of Co-doped ZnO nanorods: advancements in room temperature ferromagnetic behavior for spintronic applications. *J. Magn. Magn. Mater.* **593**, 171836. https://doi.org/10.1016/j.jmmm.2024.171836 (2024).
26. Hao, X., Xiang, D. & Jin, Z. Zn-Vacancy engineered S-Scheme zncds/zns photocatalyst for highly efficient photocatalytic H2 evolution. *ChemCatChem* **13**, 4738–4750. https://doi.org/10.1002/cctc.202100994 (2021).
27. Journal, A. I., Mishra, D., Rout, C. S., Mishra, M. & Pattanaik, A. K. Unconventional magnetism in ZnO nanorods. *Integr. Ferroelectr.* **184**, 124–128. https://doi.org/10.1080/10584587.2017.1368802 (2017).
28. Yadav, S., Rani, N. & Saini, K. A review on transition metal oxides based nanocomposites, their synthesis techniques, different morphologies and potential applications, IOP Conf. *Ser. Mater. Sci. Eng.* **1225**, 012004. https://doi.org/10.1088/1757-899x/1225/1/012004 (2022).
29. Atif, A. S., Ali, M. & Mohamed, M. Structural and optical investigation of pure and al doped ZnO annealed at different temperatures. *Opt. Quantum Electron.* **52**, 1–21. https://doi.org/10.1007/s11082-019-2158-4 (2020).
30. Makhlouf, S. A., Bakr, Z. H., Aly, K. I. & Moustafa, M. S. Structural, electrical and optical properties of Co3O4 nanoparticles. *Superlattices Microstruct.* **64**, 107–117. https://doi.org/10.1016/j.spmi.2013.09.023 (2013).
31. Farhadi, S., Pourzare, K. & Bazgir, S. Co3O4 nanoplates: synthesis, characterization and study of optical and magnetic properties. *J. Alloys Compd.* **587**, 632–637. https://doi.org/10.1016/j.jallcom.2013.10.259 (2014).
32. Khan, R., Zulfiqar, Y. & Zaman Effect of annealing on structural, dielectric, transport and magnetic properties of (Zn, Co) co-doped SnO2 nanoparticles. *J. Mater. Sci. Mater. Electron.* **27** https://doi.org/10.1007/s10854-015-4254-y (2016).
33. Shi, H. & He, X. Large-scale synthesis and magnetic properties of cubic CoO nanoparticles. *J. Phys. Chem. Solids*. **73** https://doi.org/10.1016/j.jpcs.2012.01.001 (2012).
34. Hancock, J. M. et al. Optical and magnetic properties of ZnO nanoparticles doped with co, Ni and Mn and synthesized at low temperature. *J. Nanosci. Nanotechnol.* **15** https://doi.org/10.1166/jnn.2015.9261 (2015).
35. Satpathy, S. K. et al. Influence of Gd doping on morphological, toxicity and magnetic properties of ZnO nanorods. *Mater. Today Commun.* **28**, 102725. https://doi.org/10.1016/j.mtcomm.2021.102725 (2021).
36. Rath, C. et al. Anomalous x-ray diffraction peak broadening and lattice strains in Zn1 – xCoxO dilute magnetic semiconductors. *J. Phys. Condens. Matter.* **21**, 75801. https://doi.org/10.1088/0953-8984/21/7/075801 (2009).
37. Satpathy, S. K., Panigrahi, U. K., Biswal, R. & Mallick, P. Materialia investigation on the microstructural, optical and magnetic properties of Ce doped ZnO nanorods. *Materialia* **25**, 101536. https://doi.org/10.1016/j.mtla.2022.101536 (2022).
38. Mohamed, M. et al. Optical, Magnetic, and Dielectric Investigations of, 33 (2024).
39. Elias, J., Tena-Zaera, R. & Lévy-Clément, C. Electrochemical deposition of ZnO nanowire arrays with tailored dimensions. *J. Electroanal. Chem.* **621**, 171–177. https://doi.org/10.1016/j.jelechem.2007.09.015 (2008).
40. Sakaliuniene, J., Čyviene, J., Abakevičiene, B. & Dudonis, J. Investigation of structural and optical properties of GDC thin films deposited by reactive Magnetron sputtering. *Acta Phys. Pol. A*. **120**, 63–65. https://doi.org/10.12693/APhysPolA.120.63 (2011).
41. Wilson, A. J. P. Mathematical Theroy of X-ray powder diffractometry, Cordon and Breach, New York, (1963).
42. Cahn, J. W. The impurity-drag effect in grain boundary motion. *Acta Metall.* **10**, 789–798. https://doi.org/10.1016/0001-6160(62)90092-5 (1962).
43. Novikov, V. Y. Grain growth suppression in nanocrystalline materials. *Mater. Lett.* **100**, 271–273. https://doi.org/10.1016/j.matlet.2013.03.035 (2013).
44. Gottstein, G., Molodov, D. A. & Shvindlerman, L. S. Grain boundary migration in metals: recent developments. *Interface Sci.* **6**, 7–22. https://doi.org/10.1023/a:1008641617937 (1998).
45. Dutta, S. et al. Role of defects in tailoring structural, electrical and optical properties of ZnO. *Prog Mater. Sci.* **54**, 89–136. https://doi.org/10.1016/j.pmatsci.2008.07.002 (2009).

46. Basith, N. M. et al. Co-Doped ZnO nanoparticles: structural, morphological, optical, magnetic and antibacterial studies. *J. Mater. Sci. Technol.* **30** https://doi.org/10.1016/j.jmst.2014.07.013 (2014).
47. Reddy, S., Reddy, V., Koteeswara, R. N. & Kumari, P. *Synthesis, Structural, Optical Properties and Antibacterial Activity of co-doped* (Ag, Co) ZnO Nanoparticles, 2013).
48. Kumar, S., Kumar, R. & Singh, D. P. Swift heavy ion induced modifications in Cobalt doped ZnO thin films: structural and optical studies. *Appl. Surf. Sci.* **255** https://doi.org/10.1016/j.apsusc.2009.05.005 (2009).
49. Sedky, A., Afify, N., Ali, A. M. & Algarni, H. Structural, FTIR, optical and photoluminescence investigation of Zn1-xRExO nanoparticles for optical and power operation devices. *J. Electroceram.* **49** https://doi.org/10.1007/s10832-022-00291-w (2022).
50. Mohamed, M., Sedky, A., Alshammari, A. S. & Gandouzi, M. Optical, photoluminescence and ferromagnetic properties of Ni-doped ZnO for optoelectronic applications. *J. Mater. Sci. Mater. Electron.* **32**, 5186–5198. https://doi.org/10.1007/s10854-021-05250-9 (2021).
51. Morozov, I. G., Belousova, O. V., Blanco-Andujar, C., Ortega, D. & Kuznetsov, M. V. Structural, optical, magnetic, and XPS properties of snox nanoparticles. *Solid State Sci.* **126** https://doi.org/10.1016/j.solidstatesciences.2022.106854 (2022).
52. Thamri, S., Sta, I., Jlassi, M., Hajji, M. & Ezzaouia, H. Fabrication of ZnO-NiO nanocomposite thin films and experimental study of the effect of the nio, ZnO concentration on its physical properties. *Mater. Sci. Semicond. Process.* **71** https://doi.org/10.1016/j.mssp.2017.08.017 (2017).
53. Hoseinpour, V. & Ghaemi, N. Novel ZnO-MnO2-Cu2O triple nanocomposite: facial synthesis, characterization, antibacterial activity and visible light photocatalytic performance for dyes degradation-A comparative study. *Mater. Res. Express*. **5** https://doi.org/10.1088/2053-1591/aad2c6 (2018).
54. Song, S. et al. Effect of oxygen vacancies on ferromagnetism of Cu-Doped BaSnO3. *J. Supercond Nov Magn.* **35** https://doi.org/10.1007/s10948-022-06361-y (2022).
55. Balamurugan, K., Kumar, N. H., Chelvane, J. A. & Santhosh, P. N. Room temperature ferromagnetism in Fe-doped BaSnO3. *J. Alloys Compd.* **472** https://doi.org/10.1016/j.jallcom.2008.04.096 (2009).
56. Zhang, Y. et al. Negative effect of oxygen vacancies on ferromagnetism in Ru-doped BaSnO3 materials. *Appl. Phys. Lett.* **117**, 52406. https://doi.org/10.1063/5.0005810 (2020).
57. Mohamed, M., Al–Naim, A. F., Almohammedi, A. & Sedky, A. Comparative investigation of dielectric, magnetic, and adsorption aspects of ZnO nanoparticles doped by Er or Nd. *Results Phys.* **69**, 108113. https://doi.org/10.1016/j.rinp.2025.108113 (2025).
58. Sedky, A. et al. Enhancement of mechanical and ferromagnetic properties of Cd0.4Mn0.6XO nanocomposites (X = ZnO, sno, cuo, Al2O3, Fe2O3, coo, NiO). *Mater. Sci. Eng. B.* **310**, 117737. https://doi.org/10.1016/j.mseb.2024.117737 (2024).
59. Li, Q. et al. Coexistence of superparamagnetism and ferromagnetism in Co-doped ZnO nanocrystalline films. *Scr. Mater.* **69** https://doi.org/10.1016/j.scriptamat.2013.08.007 (2013).
60. Rai, B. K., Wang, L., Mishra, S. R., Nguyen, V. V. & Liu, J. P. Synthesis and magnetic properties of hard-soft SrFe10Al 2O19/NiZnFe2O4 ferrite nanocomposites. *J. Nanosci. Nanotechnol.* **14** https://doi.org/10.1166/jnn.2014.8836 (2014).
61. Mohamed, M. et al. On the correlation between mechanical, optical, and magnetic properties of co-substituted Sn1-x-yZnxMyOz metal-oxide ceramics with M = Fe, Co, Ni, and Mn, Ceram. Int. (2024). https://doi.org/10.1016/j.ceramint.2024.02.212
62. Samanta, A., Goswami, M. N. & Mahapatra, P. K. Magnetic and electric properties of Ni-doped ZnO nanoparticles exhibit diluted magnetic semiconductor in nature. *J. Alloys Compd.* **730** https://doi.org/10.1016/j.jallcom.2017.09.334 (2018).
63. Sedky, A. & Ziq, K. A. Mechanical and magnetic properties of ZnO/Fe2O3 ceramic varistors. *Superlattices Microstruct.* **52**, 99–106. https://doi.org/10.1016/j.spmi.2012.03.021 (2012). https://doi.org/https://doi.org/
64. Ram, M. & Negi, N. S. Effect of (Fe, Co) co-doping on the structural, electrical and magnetic properties of ZnO nanocrystals prepared by solution combustion method. *Phys. B Condens. Matter*. **481** https://doi.org/10.1016/j.physb.2015.11.014 (2016).

Acknowledgements

This research has been funded by Scientific Research Deanship at University of Ha'il - Saudi Arabia through project number < < RG-24 166>>.

Author contributions

All authors have been coparticipated in all items of the manuscript, like the investigation point of the article, characterization, and measurements. Then they cooperated during the analysis and discussed the date and then wrote the text, and finally all of them reviewed the manuscript."

Declarations

Competing interests

The authors declare no competing interests.

Additional information

Correspondence and requests for materials should be addressed to A.S.

Reprints and permissions information is available at www.nature.com/reprints.

Publisher's note Springer Nature remains neutral with regard to jurisdictional claims in published maps and institutional affiliations.